PCCP

RSC Publishing

PAPER

View Article Online
View Journal | View Issue

Mechanical characteristics of human red blood cell membrane change due to C_{60} nanoparticle infiltration

Cite this: *Phys. Chem. Chem. Phys.*, 2013, **15**, 2473

Xiaoyue Zhang,[ac] Yong Zhang,[ab] Yue Zheng*[abc] and Biao Wang*[abc]

The mechanical characteristics of human red blood cell (RBC) membrane change due to C_{60} nanoparticle (NP) infiltration have been investigated in the present work. Using experimental approaches, including optical tweezer (OT) stretching and atomic force microscopy (AFM) indentation, we found that RBCs in the presence of C_{60} NPs are softer than normal RBCs. The strain–stress relations of both normal and C_{60} infiltrated RBC membranes are extracted from the data of AFM indentation, from which we proved that C_{60} NP infiltration can affect the mechanical properties of RBC membrane and tend to weaken the tensile resistance of lipids bilayers. In order to explain this experimental phenomenon, a mechanical model has been developed. Based on this model, the strain–stress relations of both normal and C_{60} infiltrated lipid bilayers are calculated with consideration of intermolecular interactions. The theoretical results are in great agreement with the experimental results. The influence of C_{60} NP concentration on the mechanical properties of RBC membrane is successfully predicted. Higher concentrations of C_{60} NPs in the lipid bilayers will lead to increased damage to the cell membrane, implying that the dosage of C_{60} NPs should be controlled in medical applications.

Received 15th August 2012,
Accepted 6th December 2012

DOI: 10.1039/c2cp42850d

www.rsc.org/pccp

1 Introduction

It is well known that the mechanical characteristics of cell membranes are significant to the biological functions of cells.[1–3] Changes in the mechanical characteristics of cell membranes can result in the progression of certain diseases. Typically, sickle cell disease is caused by a defect in the hemoglobin of human red blood cells (RBCs). The abnormality of hemoglobin alters the mechanical properties of the RBC membrane, which adversely affects its deformability and biorheology.[4] The inelastic sickle cells can easily jam-up the capillary vessels, cause the tissues surrounding the blood vessels to receive insufficient oxygen and cause severe pain. As another example, malaria is caused by the protozoa of the genus *Plasmodium falciparum*.[5] During the maturation of the parasite in the cell, the molecular constitution of its membrane is altered, then the structure of the cell cytoplasm and the shape of the cell are changed, and the cell progressively loses its function.[6,7] Generally speaking, many recent works have indicated that the mechanical information of cell membranes is an important indicator in the study of bio-processes, pathology and toxicology.

In recent years, carbon nanomaterials, including carbon nanotubes (CNTs) and carbon nanoparticles (NPs) *e.g.* C_{60} (fullerene), have been proven to possess important applications in biomedical engineering.[8,9] For example, due to their particular electrical and mechanical properties, CNTs have been considered to be a promising material for nano-biosensors and molecular carriers.[10] C_{60} (fullerene), on the other hand, has potency for induction of reactive oxygen species after photoexcitation. This property makes it possible to explore C_{60} as a new antimicrobial agent.[11] However, adverse effects and certain diseases may be caused due to the complexity of interaction between biological cells and nanomaterials.[12] For example, studies have suggested that CNTs can induce lipid peroxidation, oxidative stress and mitochondrial dysfunction in living cells. The cytotoxicity of water-soluble fullerene is the biggest obstacle to exploring it as a carrier for the delivery of drugs. Consequently, for the safety of applying nanomaterials as biomedicine, inspecting the effects of nanomaterials on living cells has become a new topic of considerable scientific interest and medical significance. Typical work such as that by Shi *et al.*[13] has investigated the mechanism of cell entry for CNTs. The article also suggests that modifying the tips of CNTs may help avoid uptake by cells and achieve material safety by design. In this work, we were especially concerned about the fact demonstrated by recent

[a] *State Key Laboratory of Optoelectronic Materials and Technologies, Micro & Nano Physics and Mechanics Research Laboratory, Sun Yat-sen University, Guangzhou, 510275, China. E-mail: zhengy35@mail.sysu.edu.cn, wangbiao@mail.sysu.edu.cn*
[b] *School of Physic and Engineering, Sun Yat-sen University, Guangzhou, 510275, China*
[c] *School of Engineering, Sun Yat-sen University, Guangzhou, 510275, China*

works that C_{60} can easily infiltrate living cells, disturb functions of cells and potentially cause nanotoxicity by changing the molecular structure of the cell membrane and organelles. Based on theoretical molecular dynamics (MD) simulations, researchers have reported the ability of C_{60} to infiltrate into the lipid bilayers.[14–17] Results of the MD simulations indicated that C_{60} particles have the ability to easily infiltrate into the lipid bilayers, stay between the lipids, and finally alter the molecular structure and interactions between lipids.[14] In fact, other recent works have also shown that C_{60} NPs might exhibit cytotoxicity in people and animals.[18–24] However, the pathogenesis of the toxicity of C_{60} NPs has not yet been made clear. Other than chemical transformation processes, *i.e.* oxidation, the cytotoxicity of C_{60} NPs results from changes in the cell membrane mechanical characteristics. Therefore, it is necessary and important to clarify any differences of mechanical properties between the cell membrane with and without C_{60} infiltration, respectively.

In this paper, the mechanical characteristics of RBCs with and without C_{60} NP infiltration have been investigated. An optical tweezers (OT) approach has been firstly used to perform stretching on integrated RBCs with and without C_{60} presence to directly investigate the effects of C_{60} NP infiltration on the mechanical properties of RBCs. In order to apply a larger load on RBCs, atomic force microscopy (AFM) was used to perform indentation on both normal and C_{60} infiltrated RBCs, and gain further data of mechanical characteristics of RBC membrane changing due to C_{60} NP infiltration. At the same time, a molecular theory has been established to explain the experimental results, and demonstrate how the C_{60} NPs affect the lipid bilayer mechanical characteristics.

2 Experimental

Preparation of RBC simples

RBCs have a relatively simple structure that readily facilitates single cell mechanical deformation experiments.[23,24] Therefore, we used human RBCs and their membrane as samples. Human RBCs were separated from the blood of a healthy donor using centrifugation. Two groups of samples were prepared, which were normal RBCs and RBCs with C_{60} infiltration. The normal RBC sample can be easily obtained by adding 20 μl RBCs into 10 ml Alsever's solution. In preparing the sample of RBCs with C_{60} presence, 5 mg C_{60} NPs were first added to 10 ml Alsever's solution. The C_{60} NPs were then uniformly dispersed in the mixture using supersonic-vibrating. Hereafter, 20 μl RBCs were added into the mixture. After quiescence under room temperature for 20 min, RBCs with C_{60} NP infiltration can be obtained. Although the quantity of C_{60} NPs in the mixture is high for the sample with C_{60} NP presence, not all the C_{60} NPs actually entered the cell membrane. Therefore, the high concentration of C_{60} NPs in the mixture is necessary.

Optical tweezer setup

For measuring the mechanical properties of an integrated cell, an approach based on OT is very useful.[6,7] The schematic diagrams of the approach are shown in Fig. 1a. A 75 mW He–Ne laser source (Coherent, Inc.) is used for laser generation. The collimated laser beam is connected to an inverted microscope (Olympus Corporation, IX71). To create a laser trap with high quality, we use a 100× oil-immersed objective with NA = 1.1 (Olympus Corporation). Two polystyrene micro-beads with a diameter of 5 μm are attached to the surface of the RBC sample. One of the beads was attached to the slip, the other bead and the cell are free standing. With the photons from the laser beam passing through the high-refractive-index dielectric bead, the change of the momentum can induce the external force on the bead, which is then "trapped" in the focal point of the laser. By trapping the free standing bead and pulling it away from the bead that sticked on the slip, the RBC sample can be stretched. The trapping force applied on the bead is determined by the laser power. Calibrated by counter flow method,[7] the maximum trapping force in our system is 70 pN. A laser filter is used to adjust the laser power, which made trapping force of the OT tunable. To acquire the mechanical properties of integrated RBC, stretch ratios S_1/S_0 under different trapping force F have been recorded, where S_0 is the original diameter of RBC and S_1 is the length of RBC after stretching. Both normal and C_{60} infiltrated RBCs have been stretched using the OT system to investigate the effect of C_{60} infiltration on the mechanical properties of integrated RBCs.

AFM indentation

AFM indentation has been widely used in biomechanics research.[25–29] In our work, this technique has been used to investigate the mechanical characteristics of RBC membranes with and without C_{60} presence. The sketch map of the AFM indentation is shown in Fig. 1b. A single layer of RBCs with or without C_{60} infiltration was placed on the piezoelectric sample stage, respectively. By moving the spherical tip to approach and press the RBCs samples at 20 nm s^{-1}, local deformation is generated on the cell surface. The resulting deflection of the cantilever tip can be calibrated to estimate the value of the applied force and indentation depth, from which the force–indentation depth (F–H) curves of the samples can be obtained for studying the mechanical properties of cell membrane.[30,31] In this work, a CSPM5500 Scanning probe microscope system (Being Nano-Instrument, Ltd.,) is used to perform AFM indentation. The piezoelectric sample stage of our AFM system has a piezoelectric coefficient of 17 nm V^{-1}. The force constant of the probe is 0.02 N m^{-1} and the curvature radius of its tip is R = 20 nm. The maximum force that can be applied on a RBC in AFM indentation is 5 nN. In total, 100 F–H curves of both normal and C_{60} infiltrated RBCs have been obtained.

3 Results and discussion

3.1 Experimental results

As shown in Fig. 2a, the data of the OT stretching experiment reveal the effects of C_{60} NP infiltration on the mechanical properties of integrated RBCs. The slope of the F–S_1/S_0 curve of RBCs with C_{60} NP presence is smaller than that of the normal one. Under the same value of force, the deformation of RBCs

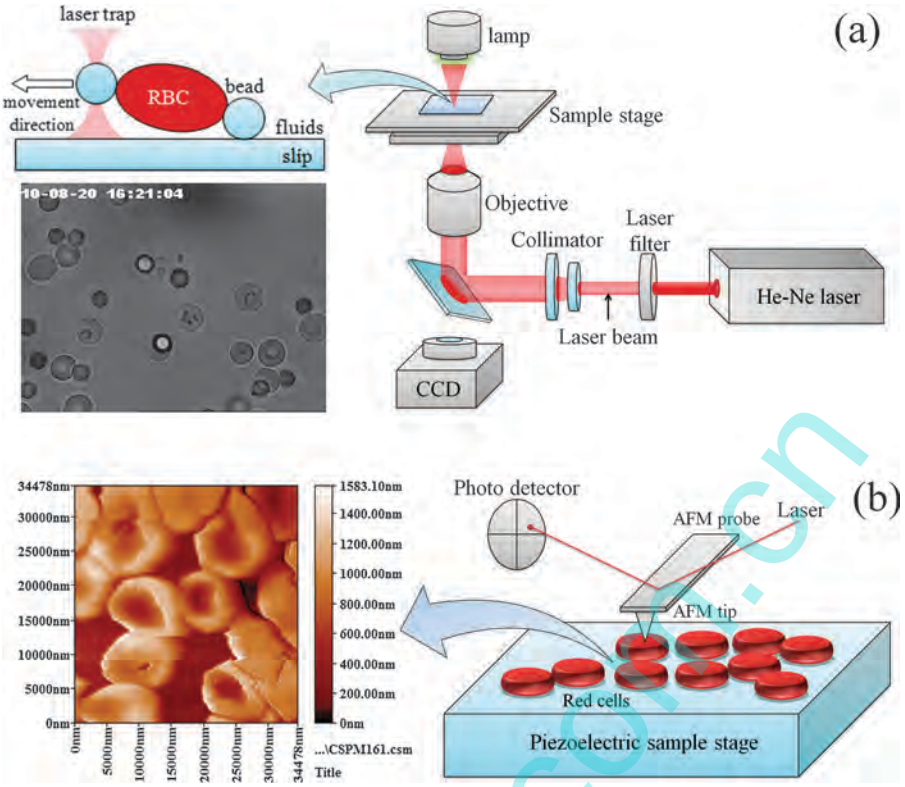

Fig. 1 (a) Diagram of stretching a RBC using OT. Two beads were attached to the surface of the RBC unspecifically, one of the beads was also attached to the slip, with the other bead and the cell remaining free standing. The free bead was trapped by the OT. By moving the beads apart, the RBC was stretched. Schematic illustration of the OT system and image of stretching a RBC observed from CCD are also shown. (b) Diagram of AFM indentation. A single layer of RBCs was placed on the piezoelectric stage. With the rise of the piezoelectric stage, a force was applied on RBC by the tip. The value of the force can be measured by recording the deflection signal of the cantilever using the laser and photo-detector. RBC samples imaged by AFM in the contact model are also shown. The biconcave shape of the RBCs is clearly seen. Among the RBCs is the flat substrate, which proves that there is only one layer of RBCs on the substrate.

with C_{60} presence is considerably larger than that of the normal one, which proves that C_{60} NP infiltration can affect the mechanical properties of RBCs and tends to weaken the tensile resistance of the cells.

The results of AFM indentation show similar phenomena. In total, 100 *F-H* curves of both normal and C_{60} infiltrated RBCs were integrated to form the results. As shown in Fig. 2b, it can be seen that the slope of the *F–H* curve of normal RBCs is greater than that of C_{60} infiltrated RBCs. The *F–H* curves reflect the samples' resistance to the tip. The greater slope in the *F–H* curves indicates that the resistance of the sample to the indentation is relatively small. Consequently, it is easy to deduce that the RBCs with C_{60} infiltration are softer than normal RBCs. It can also be seen in Fig. 2b that the *F–H* curves of C_{60} infiltrated samples have a broader distribution range. We believe that this difference is relevant to the concentration of C_{60} NPs that enter the RBC. The RBC is softer if more C_{60} NPs enter the cell.

3.2 The strain–stress relation of normal and C_{60} infiltrated RBC membrane obtained by AFM indentation

Because AFM indentation only affects the surface of RBC, and considering the simplicity of the structure of RBCs, combined with the conclusions recently reported by MD simulations,[14–17] there are reasons to conjecture that the effects of C_{60} NP infiltration on the mechanical properties of RBCs are mainly focused on the cell membrane. In order to study the mechanical characteristics of RBC membrane change due to C_{60} NP infiltration, comparing the strain–stress relations of normal membrane with that of C_{60} infiltrated membrane is essential. In this work, we manage to extract the strain–stress relations of both normal and C_{60} infiltrated membrane from the data of AFM indentation.[32] To achieve this, the cell membrane structure is considered to be a two-dimensional, continuum material,[33,34] as shown in Fig. 3a. The strain–stress relation of the two-dimensional elastic membrane can be expressed as:[35]

$$T_{ij} = 2\left(\frac{\bar{\rho}}{\rho}\right)\left[B_2\left(\frac{\partial E}{\partial B_2}\right)\delta_{ij} + \left(\frac{\partial E}{\partial B_1}\right)\beta_{ij}\right], \quad (1)$$

where $\bar{\rho}$ and ρ are the material densities in the final and initial states, respectively, E is the potential energy of the unit area, $B_1 = \lambda_1^2 + \lambda_2^2$ and $B_2 = -\lambda_1^2\lambda_2^2$ are the invariants of the two-dimensional tensor, where λ_1, λ_2 are the principal extension ratios of the membrane in x and y direction (Fig. 3b), respectively, and β_{ij} is the Finger strain tensor, which represents area change. The bending stresses are several orders of magnitude less than the membrane stresses,[36] therefore the equations of

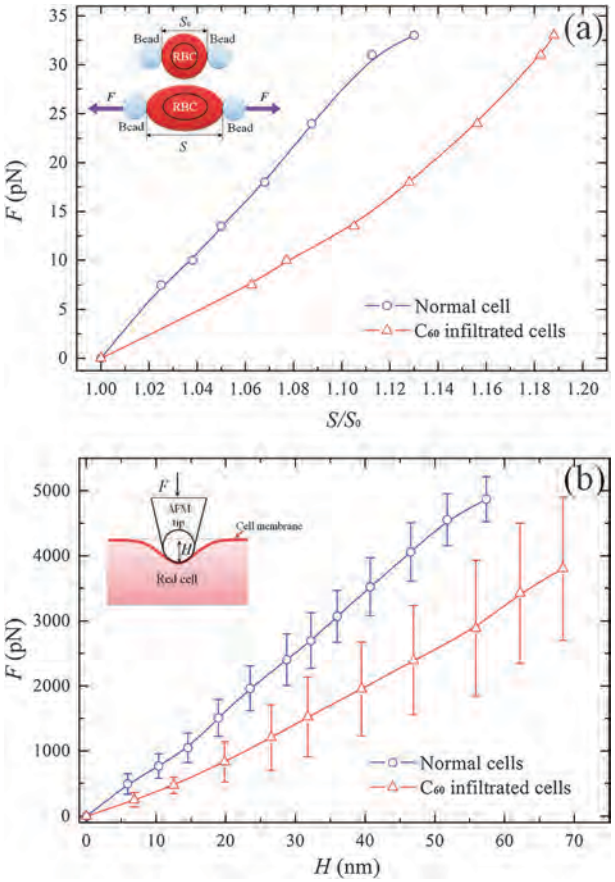

Fig. 2 (a) Force–stretch ratio curves of both normal (blue line) and C_{60} infiltrated (red line) RBCs. The slope of the curves of samples with C_{60} is smaller than the normal one, implying that C_{60} NP infiltration can affect the mechanical properties of RBCs and tends to weaken the tensile resistance of the cells. (b) *F*–*H* curves of both normal (red line) and C_{60} infiltrated (blue line) RBCs. The slope of the *F*–*H* curves of samples with C_{60} is smaller than the normal one, so the indentation depth *H* of C_{60} infiltrated RBCs is larger than that of normal RBCs under the same value of force, implying that the RBCs with C_{60} presence are softer than normal RBCs.

equilibrium for the membrane under a constant pressure load can be written as:[33]

$$\begin{cases} K_1 T_s + K_2 T_\theta = P, \\ \dfrac{\partial}{\partial s}(RT_s) + \dfrac{\partial T_{\theta s}}{\partial s} - T_\theta \left(\dfrac{\partial R}{\partial s}\right) = 0, \\ \dfrac{\partial}{\partial s}(RT_{s\theta}) + \dfrac{\partial T_\theta}{\partial s} - T_{s\theta} \left(\dfrac{\partial R}{\partial s}\right) = 0. \end{cases} \quad (2)$$

where P is the pressure difference across the membrane, and K_1 and K_2 are the principal curvatures. It can be assumed that the spheral tip applied a uniform pressure on the contact area (Fig. 3c).[37] In the contact area, the curvatures of the cell membrane are the same as that of the spheral tip, $K_1 = K_2 = 1/R$. Under such status, it is easy to know that the stress of the membrane in the contact area satisfies $T_\theta = T_s = T$ and makes the deformation status of the contact area become a uniform area deformation, which satisfies $\lambda_1 = \lambda_2 = \lambda$. In our work, the relation between T and λ of the contact area is considered to be the representative strain–stress relation of the cell membrane.

To calculate the stress T of the contact area, one can establish the *z*-direction equilibrium equation of the contact area to be $T2\pi R\sin^2\varphi_0 = F - P_0\pi R^2\sin^2\varphi_0$, where P_0 is the excess intracellular pressure and φ_0 is the tangent at the contact area boundary. Therefore, expression of the stress can be given by:

$$T = \frac{F}{2\pi R\sin^2\varphi_0} - \frac{P_0 R}{2}. \quad (3)$$

The only unknown is φ_0, which can be determined by analyzing the *x*-direction and moment equilibrium equations of isolated body ABCD (Fig. 3c) as:

$$T_b x_b \mathrm{d}\theta = P_0(R\sin\varphi_0 + x_m)H_1\mathrm{d}\theta + T(R\sin\varphi_0\cos\varphi_0)\mathrm{d}\theta, \quad (4)$$

$$T_b x_b H_1 \mathrm{d}\theta = \int_0^{H_1} P_0\left[\frac{x_b - R\sin\varphi_0}{H_1}H + R\sin\varphi_0\right]H\mathrm{d}H\mathrm{d}\theta + \int_{R\sin\varphi_0}^{x_b} P_0 x(x - R\sin\varphi_0)\mathrm{d}x\mathrm{d}\theta, \quad (5)$$

where H_1 can be calculated from $H_1 = H - R(1 - \cos\theta)$; x_b and T_b are defined to satisfy that at boundary $x = x_b$, the boundary stress T_b of the membrane has only the *x*-direction component. Therefore, x_b can be calculated from $P_0\pi x_b^2 = F$. It is hard to write an expression of $\sin\varphi_0$ as a function of H and F; however, from eqn (3)–(5), it is easy to calculate the value of $\sin\varphi_0$ corresponding to each point in the *F*–*H* curves (Fig. 1b). Thus, the stress T of the contact area can be obtained as a function of H. Establishing the relation between H and the principal extension ratios λ of the contact area is more complex; however, the relation can be approximated by power relation, $H = A(\lambda - 1)^B$. For the reason that the indentation depth H on the left of the power relation should be the same magnitude as the value of H determined from the experimental data, we approximately chose $A = 3500$ and $B = 1$ in our calculation. Although the values of parameters A and B are not absolutely precise, this hypothesis do not seriously affect the conclusion.

The strain–stress relations of both normal (blue dots) and C_{60} infiltrated RBC membrane (red and green dots) calculated from the experiment data are shown in Fig. 3d. It can be seen that the strain–stress relation of RBC membrane is significantly changed by C_{60} infiltration. The tensile resistance of RBC membrane with C_{60} infiltration is smaller than the normal one. Decrease of the tensile resistance explains why the indentation depth H of C_{60} infiltrated RBCs is larger than that of normal RBCs under the same value of force applied by the tip. Change of the strain–stress relation is direct evidence that C_{60} NPs have the ability to change the mechanical characteristics of the RBC membrane.

3.3 A molecular theory to explain how the C_{60} NPs affect the lipid bilayer mechanical characteristics

In order to explain how C_{60} NPs change the strain–stress relation of the RBC membrane, investigating the changes in the molecular structure of lipids bilayers due to C_{60} infiltration

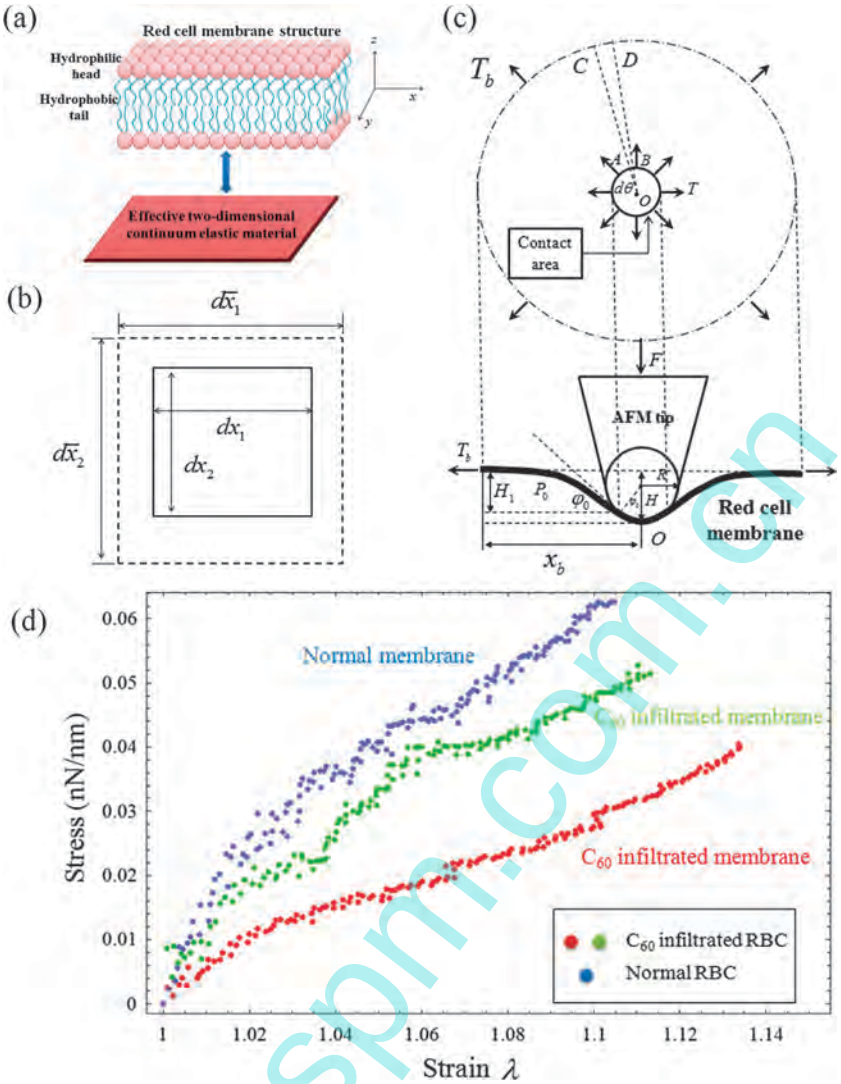

Fig. 3 (a) Schematic diagram of the effective two-dimensional continuum model. To describe the *xy*-plane mechanical behavior of the complex lipids bilayers, we simply consider the membrane to be an effective two-dimensional continuum elastic material with no thickness in the *z*-direction. (b) Schematic diagram for element side length of initial state and final state. (c) The deformation geometry of RBC membrane contact with AFM tip. In the *xz*-plane, when applying a force *F* on the tip, there is an indentation *H* in the *z* direction on RBC membrane. In the *xy*-plane, the uniform area expansion occurs on the area of the membrane in contact with the tip. (d) The strain–stress relation of the cell membrane of both normal and C_{60} infiltrated RBC. With the same stress, the strain of the C_{60} infiltrated membrane is larger than the normal one, implying that the strain–stress relation is changed.

is of first importance. According to a recent MD simulation study,[14] the infiltration of C_{60} NP into the lipid bilayer was observed and the equilibrium position of C_{60} NP in the lipids bilayers was also determined. After the C_{60} molecule entered the phospholipid bilayers, instead of the central plane of the membrane, its most probable *z*-position is $z = 1$ nm, very close to the boundaries $z = \pm 1.5$ nm, right below the head group (Fig. 4a). Due to the presence of C_{60} NPs, the relative positions of lipids are affected, which means the molecular structure of lipids bilayers is altered.

Inspired by the fact that molecular structure is crucial to the mechanical properties of cell membrane,[38] we developed a mechanical model based on intermolecular interactions to explain how the C_{60} NPs affect the mechanical characteristics of lipids bilayers. In our model, the lipid is simplified to consist of a head group and tail group, which is shown in Fig. 4a. Without the presence of C_{60}, the interaction between the two lipids can be described by the potential P_1, which has a Lennard-Jones type potential:

$$P_1(r_1) = 4\alpha_{hh}\left[\left(\frac{\beta_{hh}}{r_1}\right)^{12} - \left(\frac{\beta_{hh}}{r_1}\right)^{6}\right] + 4\alpha_{tt}\left[\left(\frac{\beta_{tt}}{r_1}\right)^{12} - \left(\frac{\beta_{tt}}{r_1}\right)^{6}\right], \quad (6)$$

where the parameters with subscript *hh* belong to the interaction between two head groups, and the parameters with subscript *tt* belong to the interaction between two tail groups; α is the depth of the potential well, β is the finite distance at which the inter-particle potential is zero, and *r* is the distance between the lipids. At $r_1 = D_1$, the potential is the minimum, and the force is zero.

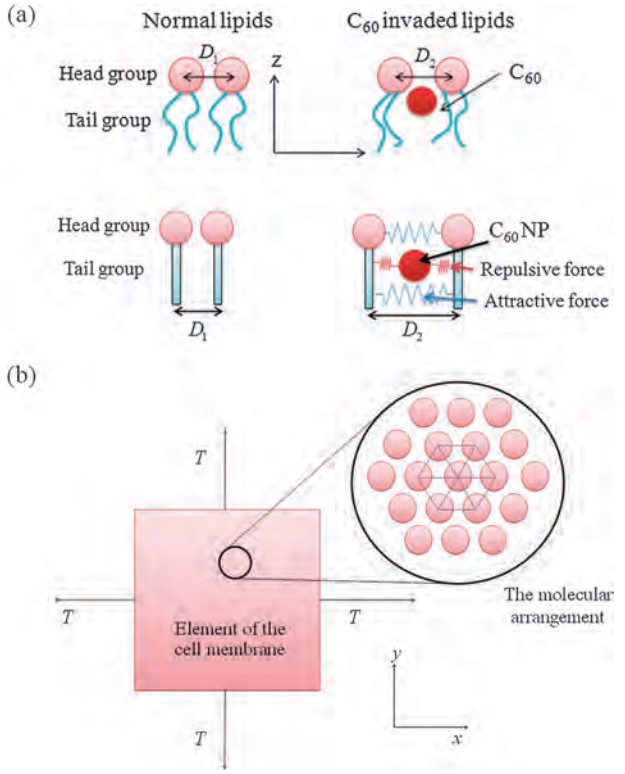

Fig. 4 (a) Schematic illustration of normal and C_{60} infiltrated lipids and the interactions between lipids and C_{60} clusters. Without the presence of C_{60}, the interactions between lipids consist of *head–head* and *tail–tail* interactions, which can be described as potential P_1. If there is a C_{60} cluster between the two lipids, it will interact with both head and tail groups and form potential P_2. Therefore, the effect of P_2 should be pulsed P_1 to form the effective potential between two lipids P_e. (b) Schematic illustration of micro-unit of cell membrane. We were only concerned with the uniform area expansion. The molecular arrangement is also shown, with the distances between neighboring lipids equivalent.

The interaction between C_{60} NP and the lipid as a function of their distance r_2 can also be described in Lennard-Jones potentials form:

$$P_2(r_2) = 4\alpha_{ch}\left[\left(\frac{\beta_{ch}}{r_2}\right)^{12} - \left(\frac{\beta_{ch}}{r_2}\right)^{6}\right] + 4\alpha_{ct}\left[\left(\frac{\beta_{ct}}{r_2}\right)^{12} - \left(\frac{\beta_{ct}}{r_2}\right)^{6}\right] \quad (7)$$

where the parameters with subscript *ch* belong to the interaction between C_{60} NP and head group, the parameters with subscript *ct* belong to the interaction between C_{60} NP and tail group.

Combining the C_{60}–lipid and lipid–lipid potentials, and noticing r_2 can be obtained by the geometrical relation and written as $r_2 = 0.5r_1$, an equivalent potential P_e of interaction between lipids with C_{60} presence can be obtained to be function of r_1 as:

$$\begin{aligned} P_e(r_1) &= P_1 + P_2 \\ &= 4\alpha_{hh}\left[\left(\frac{\beta_{hh}}{r_1}\right)^{12} - \left(\frac{\beta_{hh}}{r_1}\right)^{6}\right] + 4\alpha_{tt}\left[\left(\frac{\beta_{tt}}{r_1}\right)^{12} - \left(\frac{\beta_{tt}}{r_1}\right)^{6}\right] \\ &\quad + 4\alpha_{ch}\left[\left(\frac{\beta_{ch}}{0.5r_1}\right)^{12} - \left(\frac{\beta_{ch}}{0.5r_1}\right)^{6}\right] + 4\alpha_{ct}\left[\left(\frac{\beta_{ct}}{0.5r_1}\right)^{12} - \left(\frac{\beta_{ct}}{0.5r_1}\right)^{6}\right]. \end{aligned} \quad (8)$$

The strain–stress relation described in eqn (1) can be given by calculating the elastic potential E from P_e. The micro-unit of the cell membrane is shown in Fig. 4b. The two principal stresses satisfy $T_\theta = T_s = T$. The material is isotropic as discussed, which implies that the principal extension ratios must satisfy $\lambda_1 = \lambda_2 = \lambda$, which gives $B_1 = {\lambda_1}^2 + {\lambda_2}^2 = 2\lambda^2$, $B_2 = {\lambda_1}^2{\lambda_2}^2 = -4\lambda^4$. The molecular arrangement in the membrane element is also shown in Fig. 4b. The actual position of each lipid may not be as accurate as in the diagram; however, due to the uniformity of the membrane, it is reasonable to believe the distance between each two lipids must be almost the same. For a uniform area expansion, the principal extension ratios can always be written as $\lambda = r/D$, where D is the mean equilibrium distance between two head groups in the initial state, and r represents the mean distance between two head groups in the final state. The elastic potential can be obtained by summing all the potentials between each lipid as $E = \frac{1}{2}\sum_{i,j}^{n} P$, where the factor $\frac{1}{2}$ prevents double counting of the interaction, and where n is the total number lipids. For simplicity, in the analysis of the intermolecular interactions, we assume that long range interactions can be ignored and only short range interactions are considered.[39] A short range interaction is defined to be the interaction between two adjacent molecules and long range interaction refers to the interaction between two nonadjacent molecules. This simplification is acceptable because the short range interactions contribute the main part of the total elastic potential of the lipids bilayers. Therefore, the total elastic potential can be rewritten as $E = \frac{1}{2}6np(r) = 3np(r)$, where n of the initial state can be easily obtained by geometry as $n = \frac{2}{\sqrt{3D^2}}$. Hence the equation should be:

$$E = \frac{6}{\sqrt{3D^2}}P(r). \quad (9)$$

The density changes of lipid bilayers during the deformation can be given by $\frac{\bar{\rho}}{\rho} = M\Big/\left(\frac{M}{\lambda^2}\right) = \lambda^2$. By substituting all the equations above into eqn (1), the strain–stress relations of cell membrane with and without C_{60} molecules as a function of principal extension ratios can be theoretically given as:

$$T_n = \frac{16\sqrt{3}}{D_1^{14}\lambda^{10}}\left[-2(\alpha_{hh}\beta_{hh}^{12} + \alpha_{tt}\beta_{tt}^{12}) + D_1^6(\alpha_{hh}\beta_{hh}^{6} + \alpha_{tt}\beta_{tt}^{6})\lambda^6\right] \quad (10)$$

and

$$\begin{aligned} T_c &= \frac{16\sqrt{3}}{D_2^{14}\lambda^{10}}\left\{-2\left[(\alpha_{hh}\beta_{hh}^{12} + \alpha_{tt}\beta_{tt}^{12}) + \alpha_{ch}\left(\frac{\beta_{ct}}{2}\right)^{12} + \alpha_{ct}\left(\frac{\beta_{ct}}{2}\right)^{12}\right]\right. \\ &\quad \left. + D_2^6\left[(\alpha_{hh}\beta_{hh}^{6} + \alpha_{tt}\beta_{tt}^{6} + \alpha_{ch}\left(\frac{\beta_{ch}}{2}\right)^{6} + \alpha_{ct}\left(\frac{\beta_{ch}}{2}\right)^{6}\left(\frac{\lambda}{2}\right)^{6}\right]\right\}. \end{aligned} \quad (11)$$

eqn (10) and (11) are the strain–stress relations of normal cell membrane and C_{60} infiltrated cell membrane, respectively. However, it should be pointed out that in the derivation of eqn (11), it is assumed that all "bonds" between lipids in the

membrane are affected by C_{60} NPs. Therefore, eqn (11) describes the weakest tensile resistance of lipid bilayers due to C_{60} infiltration with highest concentration. According to our experimental results, the concentration of C_{60} NPs is one of the factors that influence the strain–stress relations. Therefore, we have also derivated the strain–stress relations to correlate with the concentration of C_{60} NP presence in the lipid bilayers. Supposing that the proportion of the number of "bonds" affected by C_{60} NPs is ω ($\omega \in (0,1)$), then because the total number of "bonds" per unit area is $\frac{6}{\sqrt{3}D^2}$, the number of "bonds" affected by C_{60} NPs is $\frac{6\omega}{\sqrt{3}D^2}$, and the number of normal "bonds" that are not affected by C_{60} NPs is $\frac{6(1-\omega)}{\sqrt{3}D^2}$. The potential energy E in eqn (1) then can be considered to contain two parts and can be rewritten as $E = E_n + E_c$, where E_n represents the total energy of normal "bonds" and E_c represents the total energy of C_{60} NP affected "bonds". Thus, eqn (1) can be rewritten as:

$$T_{c\omega} = 2\left(\frac{\bar{\rho}}{\rho}\right)\left\{B_2\left[\frac{\partial(E_n+E_c)}{\partial B_2}\right]\delta_{ij} + \left[\frac{\partial(E_n+E_c)}{\partial B_1}\right]\beta_{ij}\right\}. \quad (12)$$

where E_n and E_c can be approximately calculated as:

$$\begin{cases} E_n = \dfrac{6(1-\omega)}{\sqrt{3}D_1^2}P_1(r), \\ E_c = \dfrac{6\omega}{\sqrt{3}D_2^2}P_e(r) \end{cases}. \quad (13)$$

Therefore, eqn (11) can be rewritten to contain the information of concentration of C_{60} NP presence as:

$$\begin{aligned} T_{c\omega} &= \frac{16\sqrt{3}(1-\omega)}{D_1^{14}\lambda^{10}}\left[-2(\alpha_{hh}\beta_{hh}^{12}+\alpha_{tt}\beta_{tt}^{12}) + D_1^6(\alpha_{hh}\beta_{hh}^6+\alpha_{tt}\beta_{tt}^6)\lambda^6\right] \\ &+ \frac{16\sqrt{3}\omega}{D_2^{14}\lambda^{10}}\left\{-2\left[(\alpha_{hh}\beta_{hh}^{12}+\alpha_{tt}\beta_{tt}^{12}) + \alpha_{ch}\left(\frac{\beta_{ch}}{2}\right)^{12} + \alpha_{ct}\left(\frac{\beta_{ct}}{2}\right)^{12}\right]\right. \\ &\left. + D_2^6\left[\left(\alpha_{hh}\beta_{hh}^6+\alpha_{tt}\beta_{tt}^6+\alpha_{ch}\left(\frac{\beta_{ch}}{2}\right)^6+\alpha_{ct}\left(\frac{\beta_{ct}}{2}\right)^6\right)\left(\frac{\lambda}{2}\right)^6\right]\right\}. \end{aligned} \quad (14)$$

By comparing the theoretical strain–stress relation and experimental data of AFM indentations, the values of parameters α and β can be determined. Based on the strain–stress relation deduced by AFM indentation, choosing α_{tt} = 0.0003 nN nm, β_{tt} = 0.4 nm and $\alpha_{tt} = \alpha_{hh}$, $\beta_{hh} = 1.1\beta_{tt}$ enables eqn (10) to describe the strain–stress relation of normal lipid bilayers correctly. In determining the values of α_{ch}, α_{ct}, β_{ch} and β_{ct}, the experimental strain–stress relations of the softest membrane with C_{60} infiltration, as shown with red dots in Fig. 3d, were used as the benchmark. However, even in the softest RBC with C_{60} presence, not all "bonds" between lipids in the membrane are affected by C_{60} NPs. Therefore, the influence of C_{60} NPs on the mechanical properties of RBC membrane will be underestimated. To remedy this deviation, the parameters in eqn (7) should be chosen to make the slope of theoretical strain–stress relation smaller than the benchmark,

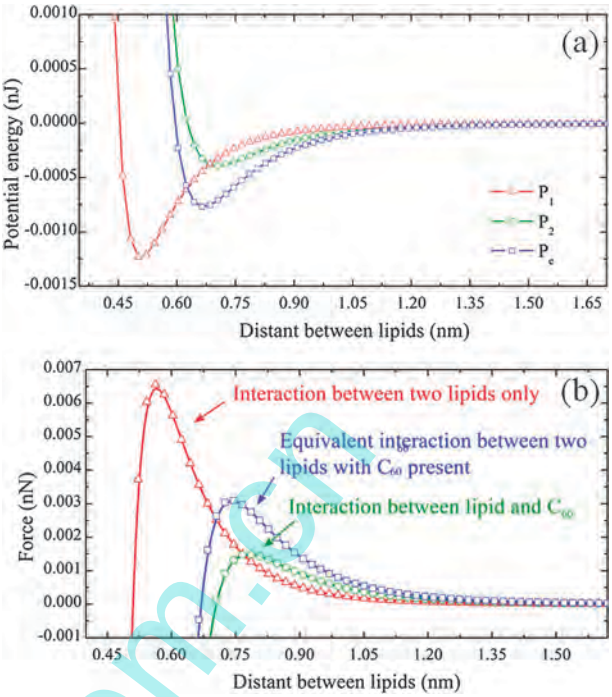

Fig. 5 (a) Comparison between P_1 P_2 and P_e. (b) Comparison of force–distance curves of interactions between lipid–lipid, C_{60}–lipid and effective interaction of lipid–lipid with C_{60} presence.

which then is chosen to be $\alpha_{ct} = 0.5\alpha_{tt}$, $\alpha_{ch} = 0.5\alpha_{hh}$, $\beta_{ct} = 0.5\beta_{tt}$ and $\beta_{ch} = 0.75\beta_{hh}$. Because $r_2 = 0.5r_1$, the parameters satisfy the condition that the forces between C_{60} NP and the head group tend to be repulsive, which is reflected in the formulation that β_{ch}/r_2 is larger than β_{hh}/r_1. The chosen parameters also reflect that tail groups tend to attract C_{60} NPs. Comparisons of the potentials and forces between normal lipids and between C_{60} infiltrated lipids are shown in Fig. 5. Three differences should be noticed. First, with C_{60} presence, the equilibrium distance between lipids increases to $r = D_2$, which will surely change the density of the cell membrane; Second, the slope of the potential decrease, which implies that the interactions between lipids are weakened. The maximal constraint force between lipids is also reduced, which influences the ultimate strength of the cell membrane. It can be considered that lipids in the cell membrane are connected with "bonds", and the presence of C_{60} NPs weakens the "bonds".

After determining the values of these parameters, the strain–stress relations of both normal and C_{60} infiltrated RBC membranes can be calculated, which are shown in Fig. 6 with lines. According to the theoretical results, the tensile resistance of lipid bilayers decreases with the increase of infiltrated C_{60} NP concentration, and the slope of the strain–stress curve is reduced to approximately 2/3 of that in normal cell membrane. The strain–stress relations induced by AFM indentation data shown in Fig. 3e are in great agreement with the theoretical strain–stress curve of the normal RBC membrane, in which 25 and 75% of "bonds" are affected by C_{60} NPs, respectively. This proves that our theory can accurately predict the mechanical characteristic changes due to C_{60} NP infiltration.

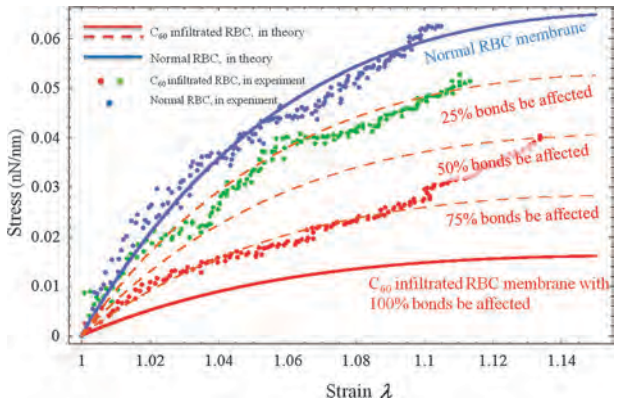

Fig. 6 The strain–stress relation comparison between normal and C_{60} infiltrated RBCs under uniform area expansion. The blue line relates to the theoretical results of normal membrane and blue dots to the strain–stress relation obtained by experiment. The red line refers to the theoretical results of lipids bilayers with 100% of "bonds" affected by C_{60} infiltration. The red dashed lines refer to the theoretical results of lipid bilayers with 25, 50 and 75% of "bonds" affected by C_{60} infiltration. The red and green dots are the experimental strain–stress relations of C_{60} infiltrated RBC membranes.

The decrease in tensile resistance implies that it may involve risk to use NPs in medical treatment with mass dosage. The effect of mass dosage of C_{60} NPs on RBC membrane might be similar to malaria, a disease resulting from merozoites change and the destruction of the molecular structure of RBC membranes[40] that causes fever and disseminated intravascular coagulation (DIC). The results also imply that the ultimate strength of the cell membrane is reduced by C_{60} NPs. The ultimate strength corresponds to the largest force the element can provide to resist the applied load. It can be seen in Fig. 6 that the ultimate stress of the cell is reduced from 0.08 nN to 0.04 nN nm^{-1} due to the infiltration of C_{60} NPs. RBCs experience different obstacles in blood circulation. If their ultimate strength decreases, many of them might dehisce in circulation. In that case, hemolytic anemia may happen, of which the consequences are serious and may be fatal. Not limited to RBCs, most human cells have a similar membrane structure; therefore, C_{60} also has the ability to change their mechanical characteristics and have different affects on their functions. For example, our results provide the explanation for the experimental results reported by ref. 22 that human skin (HDF) and liver carcinoma (HepG2) cells begin to exhibit signs of leaky membranes after 30 h of exposure to C_{60} NPs. Also, considering that the infiltration of C_{60} NPs does not depend on any receptor on a cell membrane, it is reasonable to speculate that other NPs have the same ability to infiltrate into lipid bilayers as long as they are small enough[41] and have a hydrophobic surface. However, the question of whether the infiltration of these NPs can affect the cell membrane in the same way as C_{60} still remains to be answered by further studies. So far, our parallel work suggests that the effect of NP infiltration on mechanical properties might be related to the size of the NPs.

Although there are potential risks in the medical applications of C_{60} NPs, the ability of C_{60} NPs to change the mechanical characteristics of cell membranes might also be valuable for therapies of certain diseases. In fact, it is because of its phototoxicity that C_{60} is able to be explored as an antimicrobial agent. Analogously, the mechanical properties of cell membranes are essential to the functions of bacteria or cancer cells. C_{60} NPs might provide an alternative method to kill bacteria or cancer cells without resulting in increased drug resistance by changing the mechanical properties of the cell membranes. However, the crucial issue of how to target C_{60} NPs on the right cells without disturbing healthy ones remains to be solved. So far, little work has been devoted to utilizing the ability of C_{60} NPs to change the mechanical characteristics of cell membranes, and further research is needed on these issues.

4 Conclusions

In this paper, we investigated the mechanical characteristics of human RBC membrane change due to C_{60} NP infiltration based on an experimental method combined with theoretical analysis. Results performed by OT and AFM indicate that the mechanical properties of human RBC membrane can change due to the presence of C_{60} NPs. The tensile resistance of C_{60} infiltrated RBC membrane decreases significantly. To explain this phenomena, a mechanical model based on the intermolecular interactions was developed. Based on this model, structural change of the lipid bilayers caused by the infiltration of C_{60} was discussed, the interactions among molecules were analyzed, and the strain–stress relation of the RBC membrane was derived theoretically. The theoretical results are in good agreement with the experimental data, which approve the conclusion that the mechanical properties of RBC membrane are changed by C_{60} NPs infiltration. We believe that infiltration of C_{60} NPs will make the cell membrane 'softer' and easier to break. Our results might provide an important reference to the safe application of C_{60} NPs and to the development of new therapies using NPs in bio-medical engineering.

Acknowledgements

The authors acknowledge the financial support of the National Natural Science Foundation of China (NSFC) (Nos. 10902128, 10732100, 50802026, 10972239). Y. Z. also thanks support by the Fundamental Research Funds for the Central Universities, New Century Excellent Talents in University, Research Fund for the Doctoral Program of Higher Education, Fok Ying Tung Foundation, Natural Science Funds for Distinguished Young Scholar of Guangdong Province, and Educational Commission of Guangdong Province.

References

1 G. Bao, Mechanics of biomolecules, *J. Mech. Phys. Solids*, 2002, **50**, 2237–2274.
2 G. Bao and S. Suresh, Cell and molecular mechanics of biological materials, *Nat. Mater.*, 2003, **2**, 715–725.
3 S. Suresh, Mechanical response of human red blood cells in health and disease: Some structure-property–function relationships, *J. Mater. Res.*, 2006, **21**, 8.
4 O. S. Platt, The sickle syndrome, in *Blood Principles and Practice of Hematology*, ed. R. I. Haldin, S. E. Lux and T. P. Stossel, J. B. Lippincott, Philadelphia, 1995, pp. 1592–1700.

5 B. M. Cooke, N. Mohandas and R. L. Coppel, The malaria-infected red blood cell: structuraland functional changes, *Adv. Parasitol.*, 2001, **50**, 1–86.
6 F. K. Glenister, R. L. Coppel, A. F. Cowman, N. Mohandas and B. M. Cooke, Contribution of parasite proteins to altered mechanical properties of malaria-infected red blood cells, *Blood*, 2002, **99**(3), 1060–1063.
7 C. T. Lim, M. Dao, S. Suresh, C. H. Sow and K. T. Chew, Large deformation of living cells using laser traps, *Acta Mater.*, 2004, **52**, 1837–1845.
8 J. Panyam and V. Labhasetwar, Biodegradable nanoparticles for drug and gene delivery to cells and tissue, *Adv. Drug Delivery Rev.*, 2003, **55**, 329–347.
9 E. D. Mark, C. Zhuo and M. S. Dong, Nanoparticle therapeutics: an emerging treatment modality for cancer, *Nat. Rev. Drug Discovery*, 2008, **7**, 711–782.
10 E. Bekyarova, Y. C. Ni, E. B. Malarkey, V. Montana, J. L. McWilliams, R. C. Haddon and V. Parpura, Applications of carbon nanotubes in biotechnology and biomedicine, *J. Biomed. Nanotechnol.*, 2005, **1**(1), 3–17.
11 W. H. D. Jong and P. J. Borm, Drug delivery and nanoparticles: Applications and hazards, *Int. J. Nanomed.*, 2008, **3**(2), 133–149.
12 H. C. Fischer and W. C. W. Chan, Nanotoxicity: the growing need for *in vivo* study, *Curr. Opin. Biotechnol.*, 2007, **18**, 565–571.
13 X. Shi, A. Bussche, R. H. Hurt, A. B. Kane and H. Gao, Cell entry of one-dimensional nanomaterials occurs by tip recognition and rotation, *Nat. Nanotechnol.*, 2011, **6**(11), 714–719.
14 R. Qiao, Translocation of C_{60} and its derivatives across a lipid bilayer, *Nano Lett.*, 2007, **7**(3), 614–619.
15 L. Li, H. Davande, D. Bedrov and G. D. Smith, A molecular dynamics simulation study of C_{60} fullerenes inside a dimyristoylphosphatidylcholine lipid bilayer, *J. Phys. Chem. B*, 2007, **111**, 4067–4072 4067.
16 W. E. Jirasak, B. A. Svetlana, T. Wannapong, I. M. Tang, D. T. Peter and M. Luca, Computer simulation study of fullerene translocation through lipid membranes, *Nat. Nanotechnol.*, 2008, **3**, 363–368.
17 R. Chang and J. Lee, Dynamics of C_{60} molecules in biological membranes: Computer simulation studies, *Bull. Korean Chem. Soc.*, 2010, **31**(11), 3195.
18 M. C. Powell and M. S. Kanarek, Nanomaterial health effects—part 2: Uncertainties and recommendations for the future, *Wis. Med. J.*, 2006, **105**(2), 16–20.
19 U. O. Motohiro, A. Tsukasa, W. Fumio, S. Yoshinori and T. Kazuyuki, Toxicity evaluations of various carbon nanomaterials, *Dent. Mater. J.*, 2011, **30**(3), 245–263.
20 X. Zhu, L. Zhu, Y. Li, Z. Duan, W. Chen and P. J. J. Alvarez, Developmental toxicity in Zebrafish (*Danio Rerio*) embryos after exposure to manufactured nanomaterials: Buckminsterfullerene aggregates (nC_{60}) and fullerol, *Environ. Toxicol. Chem.*, 2007, **26**, 976–979.
21 E. Oberdörster, Manufactured nanomaterials (fullerenes, C_{60}) induce oxidative stress in the brain of juvenile largemouth bass, *Environ. Health Perspect.*, 2004, **112**, 1058–1062.
22 C. M. Sayes, J. D. Fortnerz, W. Guo, D. Lyon, A. M. Boyd, K. D. Auaman, Y. J. Tao, B. Sitharaman, L. J. Wilson, J. B. Hughes, J. L. West and V. L. Colvin, The differential cytotoxicity of water-soluble fullerenes, *Nano Lett.*, 2004, **4**(10), 1881–1887.
23 S. Sen, S. Subramanian and D. E. Discher, Indentation and adhesive probing of a cell membrane with AFM: theoretical model and experiments, *Biophys. J.*, 2005, **89**(5), 3203–3213.
24 M. Dao, C. T. Lim and S. Suresh, Deformation and failure of protein materials in physiologically extreme conditions and disease, *J. Mech. Phys. Solids*, 2003, **51**, 2259–2280.
25 G. Binnig, Ch. Gerber, E. Stoll, T. R. Albrecht and C. F. Quate, Atomic resolution with atomic force microscope, *Surf. Sci.*, 1987, **189–190**, 1–6.
26 T. G. Kuznetsova, M. N. Starodubtseva, N. I. Yegorenkov, S. A. Chizhik and R. I. Zhdanov, Atomic force microscopy probing of cell elasticity, *Micron*, 2007, **38**, 824–833.
27 L. Scheffer and A. Bitler, Atomic force pulling: probing the local elasticity of the cell membrane, *Eur. Biophys. J.*, 2001, **30**, 83–90.
28 E. K. Dimitriadis, F. Horkay, J. Maresca, B. Kachar and R. S. Chadwick, Determination of elastic moduli of thin layers of soft material using the atomic force microscope, *Biophys. J.*, 2002, **82**, 2798–2810.
29 A. B. Mathur, A. M. Collinsworta, W. M. Reichert, W. E. Kraus and G. A. Truskey, Endothelial, cardiac muscle and skeletal muscle exhibit different viscous and elastic properties as determined by atomic force microscopy, *J. Biomech.*, 2001, **34**, 1545–1553.
30 *CSPM 5500 SPM User's Manual*, Being Nano-Instrument, Ltd.
31 A. Vinckier and G. Semenza, Measuring elasticity of biological materials by atomic force microscopy, *FEBS Lett.*, 1998, **430**, 12–16.
32 J. S. Field and M. V. Swain, A simple predictive model for spherical indentation, *J. Mater. Res.*, 1993, **8**(2), 297–306.
33 E. A. Evans, A new material concept for the red cell membrane, *Biophys. J.*, 1973, **13**, 926–940.
34 E. A. Evans, New membrane concept applied to the analysis of fluid shear- and micropipette-deformed red blood cells, *Biophys. J.*, 1973, **13**, 941–954.
35 W. Prager, *Introduction to Mechanics of Continua*, Ginn and Company, Boston, 1961, 188, 198, 206, 208, 209, 211.
36 Y. C. Fung, Theoretical considerations of the elasticity of red ceils and small blood vessels, *Fed. Proc.*, 1966, **25**, 1761.
37 L. H. He, N. Fujisawa and M. V. Swain, Elastic modulus and strain-stress response of human enamel by nano-indentation, *Biomaterials*, 2006, **27**, 4388–4398.
38 P. L. Yeagle, Lipid regulation of cell membrane structure and function, *FASEB J.*, 1989, **3**, 1833–1842.
39 D. C. Rapaport, *The art of molecular dynamics simulation*, Cambridge University Press, 2004, pp. 12–13.
40 T. R. David, R. Dave and W. W. Danny, *et al.* Super-resolution dissection of coordinated events during malaria parasite invasion of the human erythrocyte, *Cell Host Microbe*, 2011, **9**, 9–20.
41 S. Zhang, J. Li, G. Lykotrafitis, G. Bao and S. Suresh, Size-dependent endocytosis of nanoparticles, *Adv. Mater.*, 2009, **21**, 419–424.